HORSESHOE CHAOS IN A PERIODICALLY PERTURBED POLARIZED OPTICAL BEAM

D. DAVID, D.D. HOLM and M.V. TRATNIK [1]

Institute for Mathematics and its Applications, University of Minnesota, Minneapolis, MN 55455, USA

Received 17 February 1989; revised manuscript received 17 March 1989; accepted for publication 10 April 1989
Communicated by A.R. Bishop

The problem of a single, polarized, laser pulse propagating as a travelling wave in an anisotropic, cubically nonlinear, lossless medium is investigated as a Hamiltonian system. This Hamiltonian system describes the travelling-wave dynamics of two nonlinearly coupled complex laser modes. Invariance of the Hamiltonian function under changes of phase of the complex two-component electric field amplitude reduces the phase space to the two-sphere, S^2, on which the problem is completely integrable. The fixed points and bifurcations of the phase portrait on S^2 are studied as the beam intensity and medium parameters are varied, and homoclinic and heteroclinic connections are identified in each parameter domain. Horseshoe chaos is analytically shown to arise when the optical parameters of the medium are perturbed due to spatially periodic inhomogeneities, by using the Melnikov method. The resulting sensitive dependence on initial conditions has implications for the control and predictability of nonlinear optical polarization switching in birefringent media.

1. Introduction

Nonlinear effects in intense polarized light beams have been studied for nearly three decades, since the invention of the laser. For instance, the precession of the polarization ellipse for a laser beam in a nonlinear medium is demonstrated in ref. [1]. More recently, dynamical systems methods have begun to be applied to the study of the potentially chaotic behavior of intense travelling-wave optical pulses. For example, polarization bistability in an isotropic medium and numerical evidence for chaos in the polarization dynamics of travelling waves are discussed in ref. [2]. Interpretations of some experimental optical data in terms of chaotic behavior in travelling-wave optical pulses are also given in ref. [3]. However, a complete analysis of the polarization dynamics for travelling-wave optical pulses has remained open until now.

This paper treats optical polarization dynamics, using the Stokes description [4] for a single laser pulse propagating as a travelling wave in an anisotropic cubically nonlinear lossless medium. Hamiltonian methods are used to reduce the phase space $\mathbb{C}^2$ (the two-component, complex-vector electric field amplitude) for the travelling-wave dynamics to the spherical surface S^2 (the Poincaré sphere). Bifurcations of the phase portrait on S^2, as functions of material properties and beam intensity, are determined, and homoclinic and heteroclinic orbits connecting hyperbolic fixed points are identified. These homoclinic and heteroclinic orbits are separatrices (i.e., stable and unstable manifolds of hyperbolic fixed points) which separate regions on S^2 having different types of periodic behavior in the travelling-wave frame. Under *spatially* periodic perturbations of the medium parameters, the separatrices are shown to tangle and produce a Smale horseshoe in the Poincaré map induced from this periodic perturbation. The presence of this tangle is diagnosed via the Melnikov method, which identifies intersections of these separatrices and estimates the width of the tangled region on S^2. The analysis presented here characterizes the location of the chaotic set, or stochastic layer, on the Poincaré sphere and the dependence of its width on the material parameters, spatial modulation amplitude and wavelength, and the optical beam intensity.

[1] Permanent address: Center for Nonlinear Studies and Theoretical Division, MS B258, Los Alamos National Laboratory, Los Alamos, NM 87545, USA.

2. Problem formulation

Propagation of an optical travelling wave pulse in a cubically nonlinear medium is described by the following system of equations [5,6],

$$\mathrm{i}\frac{\mathrm{d}}{\mathrm{d}\tau}e_j=\chi^{(1)}_{jk}e_k+3\chi^{(3)}_{jklm}e_k e_l e^*_m\,, \tag{2.1}$$

where τ is the independent variable for travelling waves, j, k, l, $m=1$, 2, and the complex two-vector $\boldsymbol{e}=(e_1, e_2)^{\mathrm{T}}\in\mathbb{C}^2$ represents the electric field amplitude. The complex susceptibility tensors $\chi^{(1)}_{jk}$ and $\chi^{(3)}_{jklm}$ parametrize the linear and nonlinear polarizability, respectively. Far from resonance and in a lossless medium, the susceptibility tensors are constant and Hermitian in each $\boldsymbol{e}$–$\boldsymbol{e}^*$ pair and $\chi^{(3)}$ possesses a permutation symmetry:

$$\chi^{(1)}_{jk}=\chi^{(1)*}_{kj}\,,\quad \chi^{(3)}_{jklm}=\chi^{(3)*}_{kjml}\,,$$
$$\chi^{(3)}_{jklm}=\chi^{(3)}_{mklj}=\chi^{(3)}_{jlkm}\,. \tag{2.2}$$

Hence, we may write the system (2.1) in Hamiltonian form as

$$\partial e_j/\partial\tau=\{e_j, H\}=-\mathrm{i}\partial H/\partial e^*_j\,,$$
$$H\equiv e^*_j\chi^{(1)}_{jk}e_k+\tfrac{3}{2}e^*_j e_k\chi^{(3)}_{jklm}e_l e^*_m\,. \tag{2.3}$$

In addition, the intensity, $r=|\boldsymbol{e}|^2=|e_1|^2+|e_2|^2$, is conserved. We introduce the three-component Stokes vector, $\boldsymbol{u}$, given by (see ref. [7]) $\boldsymbol{u}=e^*_j(\sigma)_{jk}e_k$, with $\sigma=(\sigma_1, \sigma_2, \sigma_3)$, the standard Pauli matrices. The travelling wave equation (2.1) then becomes

$$\frac{\mathrm{d}\boldsymbol{u}}{\mathrm{d}\tau}=(\boldsymbol{b}+\mathbf{W}\cdot\boldsymbol{u})\times\boldsymbol{u}\,,\quad \boldsymbol{b}=\boldsymbol{a}+|\boldsymbol{u}|\boldsymbol{c}=\boldsymbol{a}+r\boldsymbol{c}\,, \tag{2.4}$$

where the constant vectors $\boldsymbol{a}$ and $\boldsymbol{c}$, and the constant symmetric tensor $\mathbf{W}$, are given by

$$\boldsymbol{a}=(\sigma)_{kj}\chi^{(1)}_{jk}\,,\quad \boldsymbol{c}=\tfrac{3}{2}(\sigma)_{kj}\chi^{(3)}_{jkll}\,,$$
$$\mathbf{W}=\tfrac{3}{2}(\sigma)_{kj}\chi^{(3)}_{jklm}(\sigma)_{lm}=\mathrm{diag}(\lambda_1, \lambda_2, \lambda_3)\,. \tag{2.5}$$

The material parameters $\boldsymbol{a}$, $\boldsymbol{c}$, and $\mathbf{W}$ are all real. According to eq. (2.5), the parameters $\boldsymbol{a}$ and $\boldsymbol{c}$ represent the effects of linear and nonlinear anisotropy, respectively. They lead to precession of the Stokes vector $\boldsymbol{u}$ with (vector) frequency $\boldsymbol{b}$. The tensor $\mathbf{W}$ is symmetric, so a polarization basis may always be assumed in which $\mathbf{W}$ is diagonal, $\mathbf{W}=(\lambda_1, \lambda_2, \lambda_3)$, in analogy to the principal moments of inertia of a rigid body.

In terms of the Stokes parameters, $\boldsymbol{u}$, the Hamiltonian function H in eq. (2.5) may be rewritten as

$$H=\boldsymbol{b}\cdot\boldsymbol{u}+\tfrac{1}{2}\boldsymbol{u}\cdot\mathbf{W}\cdot\boldsymbol{u} \tag{2.6}$$

and the equations of motion (2.9) may be expressed in Hamiltonian form as $\mathrm{d}\boldsymbol{u}/\mathrm{d}\tau=\{\boldsymbol{u}, H\}$, by using the Lie–Poisson bracket $\{F, G\}:=\boldsymbol{u}\cdot\nabla F(\boldsymbol{u})\times\nabla G(\boldsymbol{u})$ written in triple scalar product form, just as in the case of the rigid body. The intensity $r=|\boldsymbol{u}|$ is the Casimir function for this Lie–Poisson bracket. That is, r Poisson-commutes with all functions of $\boldsymbol{u}$ when the above Lie–Poisson bracket is used; so the intensity r in the Stokes description of lossless polarized optical beam dynamics may be regarded simply as a constant parameter. (See ref. [8] for discussions and references concerning Lie–Poisson brackets and their usage, for example, in the study of Lyapunov stability of equilibrium solutions of dynamical systems.)

Solving the system (2.4) when (a) two eigenvalues of $\mathbf{W}$ coincide, and (b) one or more of the components of $\boldsymbol{b}$ vanish, can be done easily for two cases which are inequivalent under cyclic permutations of indices of $\boldsymbol{u}$. In the first case, we set $\mathbf{W}=\omega\,\mathrm{diag}(1, 1, 2)$ and $\boldsymbol{b}=(b_1, b_2, 0)$; eqs. (2.4) then read

$$\frac{\mathrm{d}u_1}{\mathrm{d}\tau}=(b_2-\omega u_2)u_3\,,\quad \frac{\mathrm{d}u_2}{\mathrm{d}\tau}=(\omega u_1-b_1)u_3\,,$$
$$\frac{\mathrm{d}u_3}{\mathrm{d}\tau}=b_1u_2-b_2u_1\,. \tag{2.7}$$

Hence, a Duffing equation emerges for u_3,

$$\frac{\mathrm{d}^2u_3}{\mathrm{d}\tau^2}=Au_3(B-u_3^2)\,,$$
$$A=\tfrac{1}{2}\omega^2\,,\quad B=\frac{2H}{\omega}-r^2-\frac{2(b_1^2+b_2^2)}{\omega^2}\,. \tag{2.8}$$

The other two components of $\boldsymbol{u}$ may be determined algebraically from the two constants of motion r and H. When B increases through zero, the Duffing equation (2.8) develops a pair of orbits, homoclinic to the fixed point u_3 (see, e.g., refs. [9] and [10]). Likewise, in the second case, we set $\mathbf{W}=\omega\,\mathrm{diag}(1, 1, 2)$ and $\boldsymbol{b}=(b_1, 0, b_3)$; eqs. (2.4) then become

$$\frac{du_1}{d\tau} = -b_3 u_2 - \omega u_2 u_3 ,$$

$$\frac{du_2}{d\tau} = \omega u_1 u_3 + b_3 u_1 - b_1 u_3 ,$$

$$\frac{du_3}{d\tau} = b_1 u_2 . \qquad (2.9)$$

Hence, provided $b_1 \neq 0$, we find

$$\frac{d^2 u_3}{d\tau^2} = A' + B' u_3 + C' u_3^2 + D' u_3^3 ,$$

$$A' = b_3 (H - \tfrac{1}{2}\omega r^2) , \quad B' = \omega H - \tfrac{1}{2}\omega^2 r^2 - b_1^2 - b_3^2 ,$$

$$C' = -\tfrac{3}{2}\omega b_3 , \quad D' = -\tfrac{1}{2}\omega^2 . \qquad (2.10)$$

Thus, the polarization dynamics for this case reduces to the motion of a particle in a quartic potential, whose solution is expressible in terms of elliptic integrals. Again, the components u_1 and u_2 may be determined algebraically from the two constants of motion, r and H. We shall return to these two cases later, when we discuss the effects of perturbations. For now, these cases suffice to demonstrate that the system (2.4) possesses bifurcations in which homoclinic orbits are created.

The system of equations (2.9) further reduces the Poincaré sphere Σ_r of radius r upon transforming to spherical coordinates

$$(u_1, u_2, u_3) = (r \sin\theta \sin\varphi, r \cos\theta, r \sin\theta \cos\varphi) .$$

In these coordinates, the reduced Hamiltonian function (2.6) and the symplectic Poisson bracket on Σ_r are expressible as

$$H = \tfrac{1}{2} r^2 [(\lambda_1 \sin^2\varphi + \lambda_3 \cos^2\varphi) \sin^2\theta + \lambda_2 \cos^2\theta]$$
$$+ r \sin\theta (b_1 \sin\varphi + b_3 \cos\varphi) + b_2 r \cos\theta ,$$

$$\{F, G\} := \frac{1}{r}\frac{\partial F}{\partial \varphi}\frac{\partial G}{\partial \cos\theta} - \frac{1}{r}\frac{\partial G}{\partial \varphi}\frac{\partial F}{\partial \cos\theta} , \qquad (2.11)$$

and the equations of motion are

$$\frac{d\theta}{d\tau} = b_1 \cos\varphi - b_3 \sin\varphi$$
$$+ (\lambda_1 - \lambda_3) r \sin\theta \cos\varphi \sin\varphi ,$$

$$\frac{d\varphi}{d\tau} = b_2 - (b_1 \sin\varphi + b_3 \cos\varphi) \cot\theta$$
$$- r(\lambda_1 \sin^2\varphi + \lambda_3 \cos^2\varphi - \lambda_2) \cos\theta . \qquad (2.12)$$

The system (2.9) is completely integrable, since it is a one-degree-of-freedom Hamiltonian system. Its solutions are expressible in terms of elliptic integrals.

3. Bifurcation analysis

We now specialize to the case of a non-parity-invariant material with C_4 rotation symmetry about the axis of propagation (the z-axis), for which material constants take the form $\mathbf{W} = (\lambda_1, \lambda_2, \lambda_3)$ and $\boldsymbol{b} = (0, b_2, 0)$. (See ref. [11] for details of what follows.) We also introduce the following parameters,

$$\mu = \lambda_3 - \lambda_1 , \quad \lambda = \frac{\lambda_2 - \lambda_1}{\lambda_3 - \lambda_1} , \quad \beta = \frac{b_2}{r(\lambda_3 - \lambda_1)} . \qquad (3.1)$$

In this case, the Hamiltonian in (2.11) and the equations of motion become

$$H = \tfrac{1}{2}\mu[(r^2 - u^2)\cos^2\varphi + \lambda u^2 + 2\beta r u] + \tfrac{1}{2}\lambda_1 r^2 , \qquad (3.2a)$$

$$\frac{du}{d\tau} = \mu(r^2 - u^2)\cos\varphi \sin\varphi , \qquad (3.2b)$$

$$\frac{d\varphi}{d\tau} = \mu[\beta r - (\cos^2\varphi - \lambda)u] , \qquad (3.2c)$$

where $u \equiv r\cos\theta$. We construct the phase portrait of the system and explain how this portrait changes as the parameters in the equations vary. The fixed points of (3.2b,c) are easily located and classified, using standard techniques. We list them in table 1, for $\mu \neq 0$. The special case where $\mu = 0$, i.e., $\lambda_3 = \lambda_1$, requires a separate analysis. In that case, the right-hand side of (1.4a) vanishes identically so that the set of fixed points of the system is the circle

$$\cos\theta = \frac{b_2}{r(\lambda_2 - \lambda_1)} = \frac{\beta}{\lambda} .$$

The phase portrait depends on two essential parameters, λ and β, or equivalently, $\lambda_2 - \lambda_1$ and b_2/r. Bifurcations of the phase portrait occur when the inequality constraints in the third column of table 1 become equalities; hence we observe that the pairs

Table 1
The fixed points of system (3.2) and their types.

Fixed point	Coordinates		Constraint	Saddle	Center
F	$\varphi=0$	$\cos\theta=\beta/(1-\lambda)$	$\beta^2<(1-\lambda)^2$	$\lambda>1$	$\lambda<1$
B	$\varphi=\pi$	$\cos\theta=\beta/(1-\lambda)$			
L	$\varphi=\pi/2$	$\cos\theta=-\beta/\lambda$	$\beta^2<\lambda^2$	$\lambda<0$	$\lambda>0$
R	$\varphi=-\pi/2$	$\cos\theta=-\beta/\lambda$			
N	$\cos^2\varphi=\lambda+\beta$	$\theta=0$	–	$\beta\in(-\lambda, 1-\lambda)$	$\beta\notin(-\lambda, 1-\lambda)$
S	$\cos^2\varphi=\lambda-\beta$	$\theta=\pi$	–	$\beta\in(\lambda-1, \lambda)$	$\beta\notin(\lambda-1, \lambda)$

of fixed points (F, B) and (L, R) appear or vanish as the lines $\beta=\pm(1-\lambda)$ and $\beta=\pm\lambda$ are crossed in the (λ, β) parameter plane (see fig. 1). The (λ, β) parameter plane is partitioned into nine distinct regions separated by four critical lines that intersect in pairs at four points. Typical phase portraits corresponding to each of these regions are shown in fig. 2. Note that the phase portraits of the unperturbed system (3.2b,c) are invariant under the following discrete transformations:

$\varphi\to\varphi\pm\pi$;

$\varphi\to\varphi\pm\pi$, $\theta\to\pi-\theta$, $\beta\to-\beta$;

$\varphi\to\varphi\pm\pi/2$, $\lambda\to1-\lambda$, $\beta\to-\beta$;

$\varphi\to\varphi\pm\pi/2$, $\lambda\to1-\lambda$, $\theta\to\pi-\theta$.

Thus, as far as the configurations of critical orbits on the phase sphere are concerned, it will be sufficient to consider the quarter plane given by $\lambda<\frac{1}{2}$ and $\beta>0$, i.e., to restrict attention to regions 1, 2, 4, and 5. Although no bifurcations occur when the λ-axis ($\beta=0$ in the parameter plane) is crossed (except for $\lambda=0$, and $\lambda=1$, the set of fixed points does not change), this line is nevertheless special. Indeed, in the interval $\lambda\in(0, 1)$, i.e. within region R5, both poles are hyperbolic, each one of them being attached to a pair of homoclinic loops. When β vanishes, these homoclinic loops merge together so as to form four heteroclinic lines (and thus four heteroclinic two-cycles) connecting the north and south poles together. On the λ-axis the polarization dynamics reduces to that of the rigid body. In that case, the phase portrait consists of the poles N and S, and the four other points are located on the equator of S^2 (this configuration of fixed points distributed on the equator is obtained only on this line). Two of these, (N, S) or (F, B) or (R, L), are unstable while the other four are stable; which pair is unstable is decided by the value of $\lambda=(\lambda_2-\lambda_1)/(\lambda_3-\lambda_1)$. The pair (F, B) is hyperbolic when $0<\lambda<1$, and (R, L) are hyperbolic whenever $\lambda>1$; in each of these cases, the unstable direction is specified by the λ_i which is neither the least nor the greatest among the three.

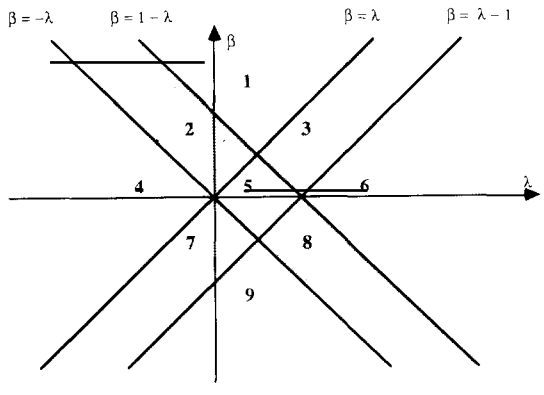

Fig. 1. The parameter plane and its bifurcation lines.

Bifurcations taking place as the beam intensity is varied are those occurring along a vertical line in the parameter plane; we present a list of the seven possible sequences (see ref. [11] for an exhaustive list of the bifurcations that may take place in the phase space when travelling along these lines):

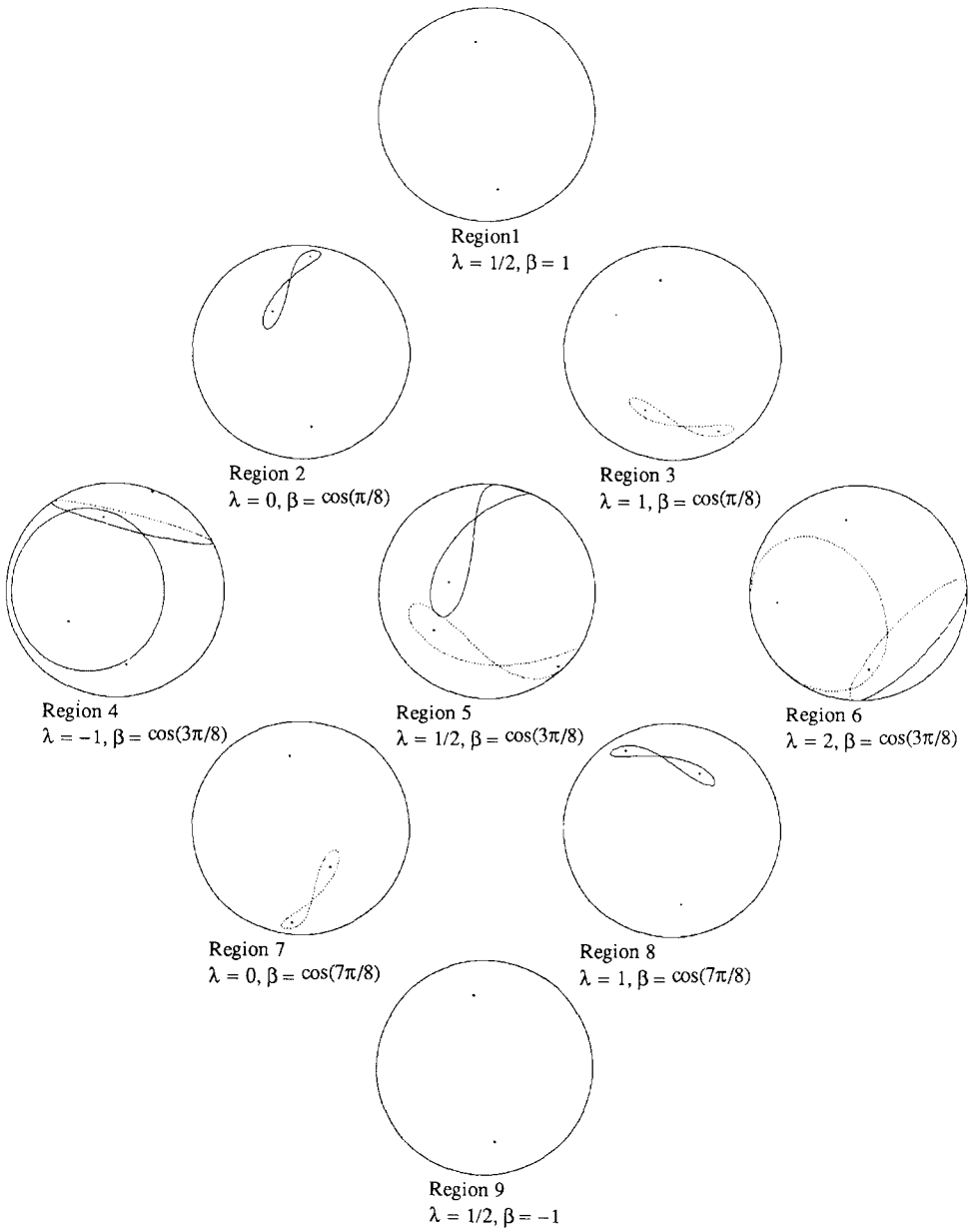

Fig. 2. Phase portraits of system (3.2).

S_1: $\lambda<0$ $R1 \leftrightarrow R2 \leftrightarrow R4 \leftrightarrow R7 \leftrightarrow R9$

S_2: $\lambda=0$ $R1 \leftrightarrow R2 \leftrightarrow R7 \leftrightarrow R9$

S_3: $0<\lambda<\frac{1}{2}$ $R1 \leftrightarrow R2 \leftrightarrow R5 \leftrightarrow R7 \leftrightarrow R9$

S_4: $\lambda=\frac{1}{2}$ $R1 \leftrightarrow R5 \leftrightarrow R9$

S_5: $\frac{1}{2}<\lambda<1$ $R1 \leftrightarrow R3 \leftrightarrow R5 \leftrightarrow R8 \leftrightarrow R9$

S_6: $\lambda=1$ $R1 \leftrightarrow R3 \leftrightarrow R8 \leftrightarrow R9$

S_7: $\lambda>1$ $R1 \leftrightarrow R3 \leftrightarrow R6 \leftrightarrow R8 \leftrightarrow R9$

4. Homoclinic chaos

In this section, we consider spatially periodic modulations of either the circular–circular polarization self-interaction coefficient λ_2 in **W** or the optical activity b_2. In each case, when the unperturbed medium satisfies the additional condition $\lambda_2=\lambda_3$, the Melnikov technique [9,10,12] leads to an analytically manageable integral for the Melnikov function, which is shown to have simple zeros. In this way, horseshoe chaos is predicted in the dynamics of the single Stokes pulse. We also discuss the physical implications for measuring this horseshoe chaos in an experimental situation.

We concentrate on the north pole $u_2=1$, $\varphi=\varphi_0$, with $\cos^2\varphi_0=\lambda+\beta$, and evaluate the conserved Hamiltonian at this point to find a relation between u and φ on the homoclinic orbit,

$$u_2=-r-\frac{2b_2}{\mu(\cos^2\varphi-\lambda)}, \tag{4.1}$$

which, when substituted into the equation of motion for φ, gives

$$\frac{\mathrm{d}\varphi}{\mathrm{d}\tau}=\mu r(\cos^2\varphi-\cos^2\varphi_0). \tag{4.2}$$

Upon integrating (4.2) we obtain (with $\tau=z+vt$, the travelling-wave variable)

$$\tan\varphi=\frac{\tan\varphi_0}{\tanh\zeta\tau}, \quad \zeta=\tfrac{1}{2}\mu r\sin 2\varphi_0. \tag{4.3}$$

Substituting this formula into (4.1) gives an analytical expression for u on the homoclinic orbit:

$$u_2=-r-\frac{2b_2}{\mu}\times\frac{1-\cos^2\varphi_0\,\mathrm{sech}^2\zeta\tau}{\cos^2\varphi_0\tanh^2\zeta\tau-\lambda(1-\cos^2\varphi_0\,\mathrm{sech}^2\zeta\tau)}. \tag{4.4}$$

We consider a periodic perturbation of the eigenvalue λ_2 and the optical activity b_2, that is,

$$\lambda_2'=\lambda_2=\epsilon_1\cos\nu z, \quad b_2'=b_2+\epsilon_2\cos\nu z, \tag{4.5}$$

where $\epsilon_{1,2}\ll 1$ and ν is the modulation frequency. Then from (2.6) the perturbation Hamiltonian is

$$H^1=\tfrac{1}{2}u_2(\epsilon_1\mu_2+2\epsilon_2)\cos\nu z, \tag{4.6}$$

and we easily calculate the Poisson bracket of this perturbation with the unperturbed Hamiltonian:

$$\{H^0,H^1\}=-\mu\sin\varphi\cos\varphi\,(r^2-u^2)u_2\cos\nu z, \tag{4.7}$$

which when formally integrated becomes the Melnikov function

$$M(\tau_0)=\mu\int_{\mathbb{P}}\sin\varphi(\tau)\cos\varphi(\tau)\,[r^2-u^2(\tau)]\times(\epsilon_1u_2+\epsilon_2)\cos[\nu(\tau-\tau_0)]\,\mathrm{d}\tau, \tag{4.8}$$

where $\tau_0=vt$. In the particular case $\lambda_2=\lambda_3$, this integral is manageable and can be found in standard tables. Hence,

$$M(\tau_0)=\frac{2\pi\nu^2}{b_2^2}\times\{r(\epsilon_1r+\epsilon_2)+\tfrac{2}{3}\epsilon_1r^2[\cos^2\varphi_0+(\nu/2b_2)^2]\}\times\mathrm{csch}\left(\frac{\nu\pi}{\mu r\sin 2\varphi_0}\right)\sin\nu\tau_0, \tag{4.9}$$

which clearly has simple zeros as a function of τ_0, implying horseshoe chaos (see, e.g., refs. [9] and [10]). When the Melnikov function has simple zeros, the dynamical evolution of a rectangular region near the homoclinic point shows (under iteration of the Poincaré map induced from the periodic perturbation) that the region is folded, stretched, contracted, and eventually mapped back over itself in the shape of a horseshoe. This horseshoe map is the underlying mechanism for chaos. As the horseshoe folds and refolds, the rectangular region of phase points initially lying near the homoclinic point develops a Cantor set structure whose associated Poincaré map can be shown to contain countably many unstable periodic motions, and uncountably many unstable nonperiodic motions. (See ref. [10] for the methods of proof of these statements and further descriptions of homoclinic tangles.)

5. Conclusions

Physically, the horseshoe chaos in the case of a periodically perturbed single Stokes pulse corresponds to intermittent switching from one elliptical polarization state, to another one whose semimajor axis is

approximately orthogonal to that of the first state, with a passage close to the unstable circular polarization state during each switch. This intermittency is realized on the Poincaré sphere by an orbit which spends most of its time near the unperturbed *figure eight* shape with a (homoclinic) crossing at the north pole (circular polarization) in fig. 2. Under periodic perturbations of either the **W**-eigenvalues or the optical activity b_2, this orbit switches deterministically, but with extreme sensitivity to the initial conditions, from one lobe of the figure eight to the other each time it returns to the crossing region near the north pole where the homoclinic tangle is located. Thus, for the one-beam problem we predict intermittent and practically unpredictable switching under spatially periodic perturbations of the material parameters, as the optical polarization state passes through a homoclinic tangle near the circular polarization state.

From considerations of the special case in which the Duffing equation (2.8) appears, one could have expected homoclinic chaos to develop for nonlinear optical polarization dynamics. Indeed, a related special case is studied numerically by Wabnitz [13] [#1]. As opposed to such numerical studies, our analytical treatment explores the bifurcations available to the polarization dynamics under the full range of material parameter variations, demonstrates that the horseshoe construct is the mechanism driving the chaotic behavior, and characterizes the location of the chaotic set, or stochastic layer, and the dependence of its width on the material parameters, modulation frequency, and optical beam intensity.

In the cases under consideration, this stochastic layer is bounded by KAM (Kolmogorov–Arnold–Moser) curves on the Poincaré sphere, inside of which the travelling-wave dynamics is regular and orbitally stable. For a given choice of beam and material parameters, these KAM curves define phase space regions where chaotic behavior (for example, sensitive dependence on initial conditions, or orbital instability) may be found, and complementary regions where chaos is absent and only regular, predictable behavior may be found.

[#1] This reference notes that eq. (2.4) also describes the classical dynamics of a single spin in a modulated magnetic field, and refers to ref. [14].

The strong dependence on intensity of the phase-space portraits reported here indicates that control and predictability of optical polarization in nonlinear media may become an important issue for future research. In particular, the sensitive dependence on initial conditions in nonlinear polarization dynamics found here to be induced by spatial inhomogeneities may have implications for the control and predictability of optical polarization switching in birefringent media. For instance, an input–output polarization experiment performed with input conditions lying in the stochastic layer for some set of material and beam parameters will show essentially random output after sufficient propagation length, depending on the amplitude and wavelength of the material inhomogeneities and the type of (transparent) material used for the experiment. Effects on optical polarization dynamics of dissipation and driving, as well as more general material descriptions and group-velocity dispersion are presently being investigated and will appear elsewhere.

Acknowledgement

This paper was written during our stay at the University of Minnesota, Institute for Mathematics and its Applications, during fall, 1988, and we wish to thank the IMA for their invitation and their hospitality. We would also like to thank S. Wiggins, A.V. Mikhailov and Y. Kodama for stimulating scientific discussions during the course of this work. Two of us (D.D. and M.V.T.) acknowledge postdoctoral fellowships from the National Science and Engineering Research Council of Canada.

References

[1] P.D. Maker, R.W. Terhune and C.M. Savage, Phys. Rev. Lett. 12 (1964) 507.
[2] K. Otsuka, J. Yumoto and J.J. Song, Opt. Lett. 10 (1985) 508.
[3] S. Trillo, S. Wabnitz and R.H. Stolen, Appl. Phys. Lett. 49 (1986) 1224.
[4] M. Born and E. Wolf, Principles of optics (Pergamon, Oxford, 1959).
[5] Y.R. Shen, The principles of nonlinear optics (Wiley–Interscience, New York, 1984).

[6] N. Bloembergen, Nonlinear optics (Benjamin, New York, 1965).
[7] D. David, D.D. Holm and M.V. Tratnik, Hamiltonian chaos in nonlinear optical polarization dynamics, Preprint LA-UR-88-1889, Los Alamos National Laboratory (1988).
[8] D.D. Holm, J.E. Marsden, T. Ratiu and A. Weinstein, Phys. Rep. 123 (1985) 123.
[9] J. Guckenheimer and P. Holmes, Nonlinear oscillations, dynamical systems, and bifurcations of vector fields (Springer, Berlin, 1983).
[10] S. Wiggins, Global bifurcations and chaos – analytical methods (Springer, Berlin, 1988).
[11] D. David, D.D. Holm and M.V. Tratnik, Chaotic dynamics in a polarized optical beam submitted to periodic and dissipative perturbations (in preparation).
[12] V.K. Melnikov, Trans. Moscow Math. Soc. 12 (1963) 1.
[13] S. Wabnitz, Phys. Rev. Lett. 58 (1987) 1415.
[14] K. Nakamura, Y. Okazaki and A.R. Bishop, Phys. Rev. Lett. 57 (1986) 5.